PHYSICAL REVIEW D
PARTICLES AND FIELDS

THIRD SERIES, VOLUME 29, NUMBER 7 1 APRIL 1984

Total cross section for electron-positron annihilation into hadron final states in the upsilon energy region

R. Giles, J. Hassard, M. Hempstead, K. Kinoshita, W. W. MacKay, F. M. Pipkin, and Richard Wilson
Harvard University, Cambridge, Massachusetts 02138

P. Haas, T. Jensen, H. Kagan, and R. Kass
Ohio State University, Columbus, Ohio 43210

S. Behrends, K. Chadwick, J. Chauveau,* P. Ganci, T. Gentile, Jan M. Guida, Joan A. Guida, A. C. Melissinos, S. L. Olsen, G. Parkhurst, D. Peterson, R. Poling, C. Rosenfeld, G. Rucinski,† E. H. Thorndike, and P. Tipton
University of Rochester, Rochester, New York 14627

D. Besson, J. Green, R. G. Hicks,‡ R. Namjoshi, F. Sannes, P. Skubic,§ A. Snyder, and R. Stone
Rutgers University, New Brunswick, New Jersey 08854

A. Chen, M. Goldberg, N. Horwitz, A. Jawahery, P. Lipari, G. C. Moneti, C. G. Trahern, and H. van Hecke
Syracuse University, Syracuse, New York 13210

M. S. Alam, S. E. Csorna, L. Garren, M. D. Mestayer, R. S. Panvini, and Xia Yi
Vanderbilt University, Nashville, Tennessee 37235

P. Avery, C. Bebek, K. Berkelman, D. G. Cassel, J. W. DeWire, R. Ehrlich, T. Ferguson, R. Galik, M. G. D. Gilchriese, B. Gittelman, M. Halling, D. L. Hartill, D. Herrup,** S. Holzner, M. Ito, J. Kandaswamy, D. L. Kreinick, Y. Kubota, N. B. Mistry, F. Morrow, E. Nordberg, M. Ogg, R. Perchonok,†† R. Plunkett,‡‡ A. Silverman, P. C. Stein, S. Stone, D. Weber, and R. Wilcke‡‡
Cornell University, Ithaca, New York 14853

A. J. Sadoff
Ithaca College, Ithaca, New York 14850
(Received 3 November 1983)

We report measurements made with the CLEO detector at the Cornell Electron Storage Ring (CESR) of the total cross section for $e^+e^-\rightarrow$hadrons at the $\Upsilon(1S)$, $\Upsilon(2S)$, and $\Upsilon(3S)$, and in the nearby nonresonant continuum. We find $R=3.77\pm0.06$ (statistical) ±0.24 (systematic) for the ratio of the nonresonant hadronic cross section to the cross section for muon-pair production at a center-of-mass total energy $W=10.4$ GeV. For the leptonic decay widths Γ_{ee} of the $\Upsilon(1S)$, $\Upsilon(2S)$, and $\Upsilon(3S)$ we obtain $1.30\pm0.05\pm0.08$, $0.52\pm0.03\pm0.04$, and $0.42\pm0.04\pm0.03$ keV, respectively.

I. INTRODUCTION

The total cross section for e^+e^- annihilation into hadrons for center-of-mass energies W between 9 and 11 GeV shows four resonant states of the $b\bar{b}$ quarkonium system. Three of these are narrow bound $^3S_1$ states, the $\Upsilon(1S)$, $\Upsilon(2S)$, and $\Upsilon(3S)$, while the fourth state $\Upsilon(4S)$ is above threshold for production of pairs of B mesons, decays into such pairs, and is much wider than the bound states. Between these resonances, in the nonresonant or continuum region, the cross section varies smoothly with energy, decreasing as the inverse square of the center-of-mass energy.

Both the resonant and continuum cross sections provide important information about quantum chromodynamics (QCD). The total cross sections and spacing of the nar-

row resonances tell us some of the properties of the $b\bar{b}$ binding potential. Similar information has been obtained about the $c\bar{c}$ system from the ψ and ψ'. However, in this case, the dynamics is more sensitive to relativistic effects than in the heavier $b\bar{b}$ case and therefore more difficult to analyze quantitatively. The Υ states are also more useful because there are three rather than two bound states. Although the form and properties of the $b\bar{b}$ potential are suggested by QCD, it must ultimately be determined empirically from the e^+e^- data. On the other hand, perhaps the most reliable prediction of QCD is the total cross section in the continuum. The measurement therefore provides a test of the validity of the theory. In this paper we report total-cross-section measurements made by the CLEO collaboration at the Cornell Electron Storage Ring (CESR) for both the narrow resonances and the continuum.

II. DESCRIPTION OF THE CLEO DETECTOR

Figure 1 shows sections of the CLEO detector perpendicular and parallel to the colliding beams. Detailed descriptions of the CLEO detector and of various components have been published elsewhere.[1] We will therefore describe the detector only briefly in this paper.

A. Magnet

A longitudinal magnetic field is produced by a 3.2-m-long, 2-m-diameter solenoid. For the data reported in this paper the solenoid made a 4.2-kG field, uniform over the volume of the tracking chambers (described below) to better than 0.5%. The radial thickness of the aluminum coil was 0.75 radiation lengths or 0.22 pion nuclear interaction lengths.

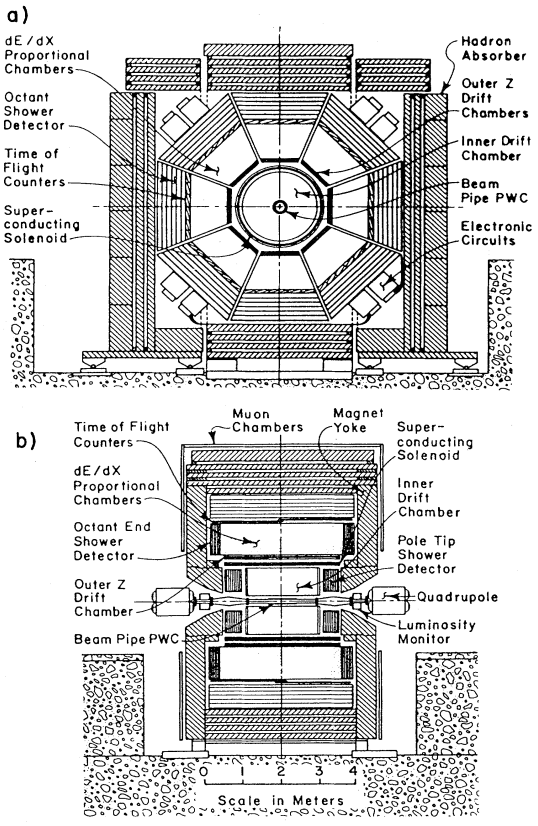

FIG. 1. End and side views of the CLEO detector.

B. Inner detector

Inside the solenoid are proportional and drift chambers for tracking charged particles, and shower counters mounted on each magnet pole tip to detect and measure the energy of photons and electrons produced at small angles to the beam.

The drift chamber is the principal device for measuring momenta of charged particles. It is in a cylindrical volume with inner diameter 0.345 m, outer diameter 1.90 m, and length 1.93 m. Sense wires form 17 concentric equally spaced cylinders of which nine have axial wires and eight have wires slanted at $\pm 2.915°$ to the longitudinal axis. The solid angle for particles which reach at least the seventh cylinder is $\Omega = 0.92 \times 4\pi$. The transverse-momentum resolution (rms) for particles which pass through 17 cylinders ($\Omega = 0.73 \times 4\pi$) was

$$(\delta p/p)^2 = [0.03p\ (\text{GeV})]^2 + 0.02^2 .$$

The first term is the curvature error due to position resolution (about 200 μm) in the drift chamber, and the second term comes from multiple scattering in the chamber. The efficiency per cylinder is typically 90%, the inefficiency coming from dead wires or electronic channels, bad calibrations, overlapping tracks, decays, and the tails of the spatial-resolution function.

The proportional wire chamber encloses the 2-mm-thick, 15-cm-diameter aluminum beam pipe. It consists of a triplet of nested cylindrical proportional wire chambers, with anode wires parallel to the beam line. The cathodes consist of 5-mm-wide strips in the form of hoops that encircle the beam. Information from the anode wires is used as a part of the fast trigger, in the event filter to reject events due to interactions of off-energy electrons with the walls of the beam pipe, and as an aid in track finding.

The pole-tip shower counters comprise one of three sets of shower counters in the CLEO detector. The other two are identified as the octant shower detector and the octant end shower detector in Fig. 1. They are all made of rectangular proportional tubes interleaved with lead sheets. Table I gives information about the construction and performance of the various shower counters.

C. Outer detector

Oustide the magnet coil in order of increasing distance from the interaction region (Fig. 1) are the following outer detector components.

(1) Three drift-chamber planes. These provide a measurement of the longitudinal coordinate for charged-particle tracks and help to identify hadrons and photons which have interacted in the coil.

(2) dE/dx chambers. These are multiwire proportional chambers operating at 45 psi, in which ionization loss of charged particles is measured. 117 samples of dE/dx are

TABLE I. CLEO detector specifications (resolutions are rms).

Charged particles: drift and proportional chambers		
	$\Omega/4\pi$	0.92
	$(\delta p/p)^2$ with $B=4.2$ kG	$[0.03p$ (GeV)$]^2+0.02^2$
	$\delta\theta$	$0.01\sin^2\theta$
	$\delta\phi$	0.002

Photons and electrons: proportional tubes and lead	Octant	Octant end	Pole tip
θ	$>55°$	40 to 50°	13 to 30°
$\Omega/4\pi$	0.47	0.11	0.12
$\delta E/\sqrt{E}$ (GeV$^{1/2}$)	0.17	0.65	0.38
$\delta\theta$	0.005	0.007	0.006
2γ separation	0.08	0.03	0.03

Hadron identification	Scintillators	dE/dx proportional chambers	
$\Omega/4\pi$	0.56	0.56	
Resolution	400 psec	5.8%	
p (GeV) for π/K	<1.0	<0.7	
p (GeV) for K/p	<1.7	<1.2	
p (GeV) to traverse coil	$\pi>0.2$,	$K>0.4$,	$p>0.6$

Muon identification: drift chambers		
	$\Omega/4\pi$	0.78
	E (GeV) to traverse iron	1 to 2

measured over a total path length of 79 cm. The truncated mean resolution (rms) is 5.8%. This measurement together with the momentum measurement in the drift chamber provides particle identification over the momentum ranges shown in Table I.

(3) Time-of-flight scintillation counters. The counters are located at about 2.3 m from the interaction regions and have a time resolution of 400 psec. Time-of-flight measurements provide an independent technique for particle identification. The scintillation counters are also used in several of the trigger options.

(4) Electromagnetic shower counters. These are the principal shower counters of the detector. They cover a solid angle $\Omega=0.47\times4\pi$ and are essential for both electron and neutral-pion identification. They are used in the trigger, and provide the most reliable absolute measure of luminosity.

The four components discussed thus far are located outside the coil and are assembled in octants. Each octant is a structural unit which includes all its associated electronics.

(5) Muon detector. The iron of the magnet is part of the hadron absorber for the muon detector. Drift chambers are located at various depths in the iron to detect penetrating charged particles. Some chambers are mounted directly on the magnet yoke and others are on four movable carts carrying additional iron. These carts are withdrawn for access to the octants.

Table I provides performance data for the various components of the detector.

D. Luminosity monitor

Surrounding the beam pipe at a distance of 2.0 m on each side of the interaction point are four scintillator telescopes, which detect small-angle elastic (Bhabha) e^+e^- scatters. Each telescope consists of two scintillators followed by a lead-scintillator sandwich array 13 radiation lengths thick. Coincidences between the scintillators in one telescope and the corresponding one on the opposite side of the interaction point define back-to-back electron-positron pairs. The scintillators cover the range 39 to 70 mrad in scattering angle. For any data run the ratio of the number of coincidences to the QED Bhabha-scattering cross section defines the time-integrated beam luminosity.

III. METHOD OF MEASUREMENT OF R IN THE CONTINUUM

The nonresonant continuum total cross section for e^+e^- annihilation into hadron final states is usually expressed as a ratio R, divided by the QED cross section for production of muon pairs; that is,

$$R=\sigma_{\rm had}/\sigma_{\mu\mu}\ .$$

The hadronic cross section is the number N of events detected and selected as hadronic, divided by the integrated luminosity $L=\int \mathscr{L}\,dt$, and corrected for the fraction of misidentified background events β, the detector acceptance ϵ (including geometric apertures, hardware performance, trigger and selection efficiencies), and radiative effects δ. Therefore,

$$R = N(1-\beta)/[\epsilon L(1+\delta)\sigma_{\mu\mu}] .$$

N, β, ϵ, and even $1+\delta$ all depend on the criteria used to select hadronic events: properties of the detector, trigger requirements, preanalysis event filter, reconstruction routines, trigger smoothing cuts, and special cuts to remove background contamination. The backgrounds are cosmic rays, beam-gas and beam-wall collisions, photon-photon collisions (i.e., $e^+e^- \to e^+e^- X$), and QED processes (mainly $e^+e^- \to \tau^+\tau^-$). They occur at a rate much larger than hadronic annihilations.

Stringent cuts on multiplicity, visible energy, vertex, and timing can significantly reduce or even eliminate the background fraction β, but will also cause good events to be lost, lowering N, and necessitating a more careful calculation of the acceptance ϵ. Such a calculation involves a computer simulation of the detector and selection criteria operating on events generated by a Monte Carlo program mimicking the real physical processes of hadron production. The acceptance ϵ is therefore model dependent and thus introduces a systematic uncertainty in the measurement of R.

Loose cuts, on the other hand, although increasing the number of selected events and improving the efficiency (making it less model dependent), cause a larger contamination by backgrounds, some of which can be impossible to measure or calculate reliably. The selection criteria must therefore be a compromise chosen to minimize the overall error in R arising from errors in N, β, and ϵ. Actually, we have used various sets of event-selection criteria in the analysis, determining N, β, ϵ, and $1+\delta$ for each set. The consistency of the resulting values of R is a test of the reliability of the procedure.

IV. EVENT-SELECTION CRITERIA

The events accepted as candidates for e^+e^- annihilation into hadrons are selected in several successive stages.

A. The hardware trigger

The beams intersect in the center of the detector 400 000 times per second. An appreciable fraction of these beam crossings are accompanied by a signal in several of the 20 000 data channels, representing ionization collected by various drift chamber or proportional chamber wires, or scintillation counters. It would be prohibitively time consuming to read out, record, and analyze all of these signals, nor is it necessary. We rely on a sophisticated trigger system to decide whether there might be an interesting event to be saved.

Five components of the CLEO detector provide signals to the trigger system: the inner cylindrical proportional chamber surrounding the beam pipe, the large cylindrical drift chamber, the time-of-flight scintillation counters, the electromagnetic shower detectors arranged in octants, and the shower detectors mounted on the magnet poles. Charged-particle triggers are obtained from the fast track-segment processor, or TSP. This hardware processor reads in the output of groups of nearby sense wires in the proportional and drift chambers. If any wire in a group has detected ionization above a minimum level, a hit is recorded. The hits feed into four TSP channels depending on the radius of the cylinder where they originate. Channel 1 receives data from the three cylinders of the inner proportional chamber, and each of channels 2 through 4 receives data from three successive cylinders of axial wires in the drift chamber.

The TSP searches within each channel for track segments, a segment being defined as two or three hits in the three successive cylinders within an azimuthal range of 24°. For each of the four channels the number of such segments found is used to set two latches, whose output, along with latches from the time-of-flight and calorimeter systems, are then coded into address words which access locations in the main decision memory of the CLEO trigger system. This is a hardware lookup table which can be programmed by the experimenter to define the addresses which correspond to valid triggers. If a valid trigger is found, the data channels are not reset and the data readout is begun. Since the whole decision process requires only 1.5 μsec, it is possible to reset the data channels in time for the next beam crossing (occurring every 2.6 μsec) in case no valid trigger is satisfied. This programmable system permits substantial flexibility and redundancy in defining the trigger requirements. We describe the most common configuration with the help of a shorthand notation TSP($n_1 n_2 n_3 n_4$), where n_i refers to the minimum number of track segments required in the ith TSP channel. Typically, either one of the following two conditions constituted a valid trigger for hadronic events.

(1) TSP(3321), TSP(3312), TSP(3222), or TSP(2322); and hits in at least two octants of time-of-flight scintillators within 110 nsec of the beam-crossing time.

(2) Any two TSP segments, and hits in two opposite time-of-flight half-octants.

Condition (1) was the principal trigger for hadronic events. Condition (2) was designed to detect muon pairs; about 85% of the hadronic events pass it as well. Several other trigger conditions were also enabled. These were optimized for QED processes and for events with a large neutral-energy fraction, and are of no relevance for our measurement of R. With these conditions the total trigger rate was generally between 1 and 2 Hz.

The CLEO trigger as described above is sensitive to events with a charged multiplicity of at least three, provided at least two charged particles are within the 50% solid angle covered by the time-of-flight scintillators and have sufficient range to penetrate the solenoid coil. Events with just two charged tracks can trigger only if the two tracks are nearly collinear and hit the time-of-flight counters, or at least one particle (charged or neutral) deposits more than 1 GeV in the octant shower-detector system, covering about 50% solid angle. An event with no triggerable charged particles can be recorded only if more than 1 GeV of energy is deposited in two octants or ends of the shower-detection systems. It is unfortunately not possible to run the CLEO detector using an unrestricted two-charged-particle trigger, without an unacceptable background rate.

B. Preanalysis filter

The track-finding program which reconstructs tracks and determines momenta from the data of the cylindrical drift chamber requires on the average about one second of computing time (on a DEC KL-10 computer) per hadronic event. Many background events can be eliminated in much less computation time, however, on the basis of a few simple data checks.

(1) The TSP latches recorded for the event must satisfy the TSP(3333) condition, which is more restrictive than any TSP requirements used in the hardware trigger. This smooths variations due to the use of different trigger combinations during the data running. It is also extremely effective in the elimination of background, particularly $e^+e^-\gamma$ final states.

(2) Two time-of-flight scintillators must register hits within a window of 75 nsec. This is a narrower cut than the hardware trigger requirement used for conditions (1) and (2).

(3) The event must contain at least 250 MeV of shower energy in the outer electromagnetic calorimeters.

(4) The event must not be classified as a "beam-wall" event originating from a collision of a stray beam particle with the beam pipe wall. This classification is accomplished by the inner proportional chamber surrounding the beam pipe. An event is *not* a beam-wall event if (a) there exist hits in all three cylinders lining up radially to within 1.5° in azimuth and (b) at least one track is found passing within 1.5 mm of the interaction point. If an event contains more than 50 hits in the inner chamber, an angular region of $\pm 15°$ centered on the direction of the center of the storage ring (where most beam-wall events have many hits) is excluded from the calculation of the first criterion.

C. Postanalysis cuts

The CLEO data-reduction program reconstructs in three dimensions the charged-particle tracks from the cylindrical drift-chamber data, determining the momentum components for each charged track produced in its sensitive range, roughly $30° < \theta < 150°$ and $p > 100$ MeV/c. Using data from the detector components outside the solenoid coil, it also reconstructs photon showers over about 80% of the full solid angle, and identifies e, μ, π, K, and p within favorable momentum and angle ranges. Only the drift-chamber results, however, are used in the selection of analyzed events to be included in the calculation of the total cross section for hadronic annihilation. The drift-chamber efficiency is more reliably modeled in simulations of its performance on Monte Carlo generated events and its properties were more constant over the period of the experiment, compared with the outer detector components.

In order to be accepted as a beam-beam annihilation the charged tracks in an event must be consistent with a vertex within 2 cm of the beam line, with a longitudinal coordinate (z) less than 8 cm from the nominal interaction point.

Uncertainties in the calculation of acceptance are minimized by basing postanalysis cuts on detected charged-particle multiplicity and charged energy. The definition of charged multiplicity used at this stage counts only tracks which are found to originate from the interaction point, and excludes tracks from recognized photon conversions and neutral particle decays. We have carried out the analysis with minimum-multiplicity cuts of five, six, and seven charged tracks, the lower limit of five being chosen to suppress the background of $e^+e^-\to\tau^+\tau^-$ events. Note that these multiplicity cuts applied to the reconstructed event data are more restrictive than either the trigger conditions or the preanalysis TSP(3333) requirement.

Charged energy is defined here as the energy measured in the cylindrical drift chamber, under the hypothesis that all particles have the pion mass. We require that an accepted hadronic event have at least 3 GeV of measured charged energy, and we also consider subsamples of events with energies above 4 and 5 GeV.

V. ACCEPTANCE

The average probability that a hadronic event will pass all the event-selection criteria is most reliably calculated stage by stage, but in reverse order. That is, we use a Monte Carlo event simulation first to determine what fraction will pass the final and most restrictive requirements, the charged multiplicity and energy cuts. Then for the subsample of Monte Carlo events which pass these cuts, we determine the fraction which pass the preanalysis filter, and finally the fraction of those which satisfy the hardware trigger conditions. In this order the major event losses occur in the first step, where the selection criteria are least dependent on subtleties of the performance of the detector and can be calculated with minimum systematic uncertainty. Events which pass these rather restrictive cuts have high efficiency to survive the preanalysis and trigger requirements, which otherwise would introduce serious uncertainties because of their more intimate dependence on the less precisely known properties of the detector. For example, one does not have to worry about the rather indeterminate trigger efficiency for two-track events; such events are excluded by our postanalysis multiplicity cut.

A. The event generator

The Monte Carlo program used to simulate continuum production of hadrons in e^+e^--annihilation-generated jet-like events by use of a modified Field and Feynman[2] scheme for fragmentation of primary quark-antiquark pairs produced with a probability proportional to the square of the quark charge. The primary pair defined an axis in space, the jet axis, which was preserved throughout the hadronization chain. Subsequent quark-antiquark pairs were generated with a Gaussian distribution of transverse momentum having a root-mean-square value of 350 MeV/c. Each generated antiquark combined with the quark from the preceding generation to form a meson. Baryon production was not included. The spin of each meson was chosen randomly, either zero or one with equal probability. The transverse momentum of the meson was

the vector sum of the quark and antiquark transverse momenta. Finally, the longitudinal momentum of the meson was determined using the Field-Feynman fragmentation function $f(z)$.[2] The variable z is the $E+p_{\text{long}}$ of the meson, divided by that for the whole jet, and $f(z)$ gives the probability (per unit z) to be assigned to the created meson. Energy and momentum are conserved at each step of the chain. The model allows gluon bremsstrahlung, the fragmentation of the gluon proceeding similarly to quark fragmentation.

B. Detector simulation

The Monte Carlo program tracked each produced particle through a simulation of the CLEO detector, taking account of bending of charged particles in the solenoid field, ionization energy loss and Coulomb scattering by charged particles, radiation by electrons, Compton scattering and pair production by photons, nuclear absorbtion, and decays. Secondary particles from radiation, pair production, and decay were also tracked. The calculation was carried through in detail for the tracking chambers inside the solenoid, including the simulation of raw data with the known sense-wire efficiencies and resolutions. In the outer detector simplified algorithms were used, taking account only of the geometry and the generalized performance of the detector modules, since a detailed following of the history of each particle would have been rather time consuming and unnecessary for the acceptance calculation.

The simulated data, including trigger information, addresses of hit sense wires in the tracking chambers inside the coil, digitized pulse heights from the annular cathode strips of the inner proportional chamber, and digitized drift times from the cylindrical drift chamber, were analyzed just as if they were real data events, in order to determine what fractions pass the various criteria listed above for hadronic annihilation events.

C. Tests of the validity of the Monte Carlo program

It would of course be useful to know if the simulated event generator correctly gave the fraction of events which would not be accepted by our hadronic event criteria. Unfortunately, there is no way to check experimentally the predictions of our model for the probability of undetectable events. The best we can do is (a) ensure that the predicted raw distributions in multiplicities, momenta, and event shapes for the detectable events agree with our data and (b) choose event-selection criteria which minimize the sensitivity to the unknown properties of the model. We have already discussed the optimization of the event-selection criteria. The agreement between the Monte Carlo simulation and our data is demonstrated by distributions in charged multiplicity (Fig. 2), inclusive charged-particle momenta (Fig. 3), sphericity,[3] thrust,[4] and the R_2 ratio of Fox-Wolfram moments[5] (Fig. 4). Note that these are distributions as seen by the real or simulated CLEO detector, uncorrected for acceptance; they are not directly comparable with predicted spectra or corrected results from other experiments. They do, however, provide a basis for estimating the systematic error in the event acceptance ϵ.

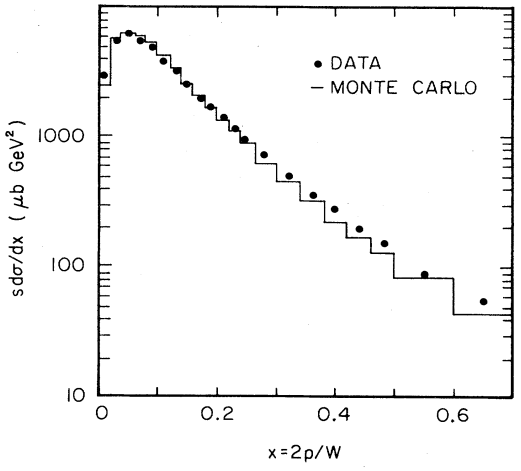

FIG. 3. The uncorrected inclusive charged-particle momentum spectrum observed in the nonresonant continuum (points) compared with the Monte Carlo simulation (histogram).

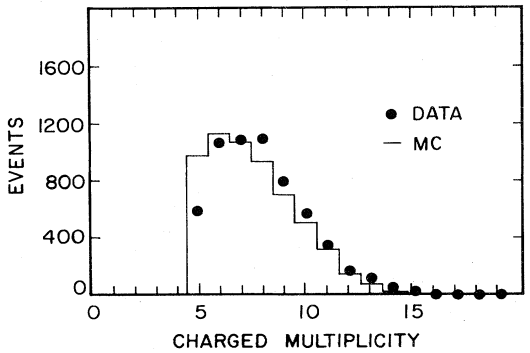

FIG. 2. The uncorrected charged-particle multiplicity distribution observed in the nonresonant continuum (points) compared with the Monte Carlo simulation (histogram).

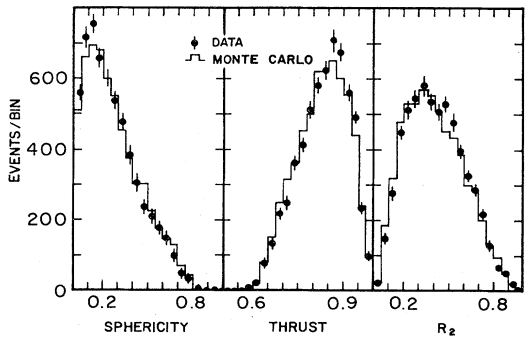

FIG. 4. Uncorrected distributions in sphericity, thrust, and R_2 (see text) observed in the nonresonant continuum (points) compared with the corresponding Monte Carlo spectra (histograms).

TABLE II. Calculated hadronic event acceptance for various postanalysis cuts on observed charged multiplicity n and energy E.

min n	min E (GeV)	Postanalysis[a]	Preanalysis filters 2,3,4[b]	Preanalysis filter 1[c]
5	3	0.730	0.962	0.905
6	3	0.633	0.970	0.920
7	3	0.500	0.978	0.942
5	4	0.638	0.964	0.901
6	4	0.565	0.972	0.918
7	4	0.457	0.979	0.939
5	5	0.497	0.966	0.909
6	5	0.449	0.974	0.927
7	5	0.373	0.980	0.948

[a]Monte Carlo statistical error is ± 0.007.
[b]For events which pass the postanalysis cuts.
[c]For events which pass the postanalysis cuts and the other preanalysis requirements.

D. Acceptance of the postanalysis cuts

Table II shows the calculated acceptance for continuum hadronic annihilation events for each combination of the three postanalysis cuts in detected charged multiplicity and the three cuts in visible charged energy. The net acceptance ϵ runs from 37% for the most restrictive combination to 73% for the least. We assign a systematic error of 3.2% for the effect of the postanalysis cuts in visible charged multiplicity and energy. It was estimated by noting the effect of making variations in the Monte Carlo input assumptions which did not significantly alter the agreement of the distributions compared with data.

E. Acceptance of the preanalysis filter

(1) The acceptance for the TSP(3333) requirement is a product of the efficiency of the proportional and drift chambers to record the required hits on charged-particle tracks and the efficiency of the track-segment processors once the hits are reported to it. Efficiencies in the first category are calculated from the individual cylinder efficiencies of 80 to 98% in the proportional and drift chambers. These cylinder efficiencies are measured by observing well fit muon-pair events and noting which of the cylinders of wires should have registered a hit but did not. We determine the inefficiencies introduced by the TSP circuitry by examining clean Bhabha-scattering events. We simulate the TSP(3333) decision algorithm using the actual data hits and compare with the recorded TSP results. The efficiencies derived are at least 95% for all four TSP channels, with an uncertainty of 1.2% coming from counting statistics in the data samples used to measure them.

(2) The requirement that two time-of-flight scintillators be hit within 75 nsec is difficult to model reliably, since the actual scintillator data are contaminated by noise and cosmic rays. A visually scanned sample of events in fact shows an average of two more scintillator hits per event than does a corresponding Monte Carlo sample. Fortunately, the error introduced by the noise difference between the data and the Monte Carlo simulation must be less than the effect (3.5%) on the Monte Carlo acceptance caused by eliminating the time-of-flight requirement altogether. To account for the noise we increase the Monte Carlo acceptance result by 2.0% and assign a systematic error of 1.5%.

(3) A visual study of a sample of real hadronic events without the preanalysis filtering shows that all but 0.3% of the events which satisfy the TSP(3333) requirement (preanalysis filter 1) also satisfy the requirement of at least 250 MeV recorded in the shower chambers. We therefore ignore this requirement in the acceptance calculation.

(4) Of all the Monte Carlo events satisfying the analysis cuts on visible multiplicity and energy, we find none which classify as beam-wall events. We therefore assign an acceptance of $(100^{+0}_{-1})\%$ for this stage of the event selection.

Table II shows the preanalysis acceptance factors for the various choices of analysis cuts on multiplicity and energy. We estimate the contribution to the systematic error in the acceptance at 2.2%. Since the preanalysis and postanalysis requirements are more stringent than any of the hardware trigger conditions, we can ignore any additional effect of trigger acceptance. Figure 5 shows the acceptance factors implied by the various event-selection requirements in actual time order.

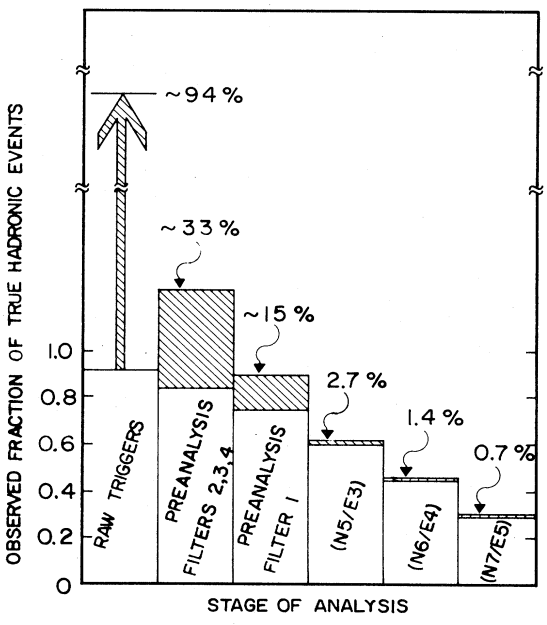

FIG. 5. Fraction of hadronic annihilation events surviving each stage of the analysis (in normal order). Since the net acceptance is actually calculated stage by stage in reverse order, the numbers here are only estimates and do not match those in the text. The cross-hatched areas show the background contamination.

VI. BACKGROUNDS

A. Beam-gas collisions

For each data run we subtract the contribution to the event sample due to interactions of beam particles with the residual gas atoms. The fraction to be subtracted is determined from the measured distribution of event vertices along the z axis, the beam line. Events with a vertex more than 12 cm but less than 30 cm from the interaction point are taken to be of beam-gas origin, and are subtracted proportionally from the number of events with vertices less than 8 cm from the interaction point (required of beam-beam collision events). Since the fraction subtracted is less than 1%, we neglect any possible effect on the acceptance for good events.

B. Beam-wall collisions, cosmic rays, and QED processes

These categories of events have distinctive features which make them easily identifiable by visual inspection. We have scanned a sample of 911 events which passed all criteria for hadronic annihilations except the postanalysis cuts were not applied. We identified 16% as beam-wall collisions, 11% as $e^+e^-\gamma$ radiative Bhabha scatters, 3% as misidentified muon pairs or cosmic rays, $<1\%$ as probable τ pairs, and $<1\%$ as probable two-photon-collision events. We conclude that the data sample without postanalysis cuts is contaminated with about 30% background. This situation improves dramatically after we impose the postanalysis requirements on charged multiplicity and energy. Only 13 beam-wall events pass the least restrictive combination of multiplicity and energy cuts; the other backgrounds make up less than 0.5% of the surviving events. From the scanning uncertainties and the statistical errors we estimate a systematic uncertainty of 1.8% in the resulting background fractions.

C. Hadronic decays of τ pairs

Nonleptonic decays of τ's are strongly suppressed by our multiplicity and energy cuts, but the contribution of the remainder must be evaluated by Monte Carlo simulation, taking into account the known branching ratios[6] and the properties of the detector. The contamination in the hadronic annihilation sample from this source is calculated to be less than 0.5%, with an estimated error of 0.3%.

D. The two-photon-collision process

The inelastic scattering of electron and positron, $e^+e^-\rightarrow e^+e^-+$hadrons, is essentially hadron production by the collision of two virtual photons, one emitted by each of the incident electron and positron. Usually the scattered electron and positron escape undetected at small angles inside the beam pipe, leaving the hadron final state with a net momentum along the beam direction and a total visible energy considerably less than the original collision energy W. Although the total cross section for this process is comparable to the desired hadronic-annihilation cross section, its effect on the accepted event rate should be considerably reduced by the postanalysis cuts on visible multiplicity and energy. Indeed, Monte Carlo simulation of the two-photon-collision events indicates that the number surviving our cuts should be insignificant, although not enough is known about the process to make a completely reliable calculation. We will neglect this as a source of background and use the consistency of the measurements of R with different postanalysis multiplicity and energy cuts as a check of the validity of the procedure. We will see that although the two-photon Monte Carlo model predicts a factor of 1.5 increase in the rate of surviving two-photon events when the visible energy threshold is reduced from 5 to 3 GeV, there is no statistically significant change in our measured R value.

Our background estimates assuming various postanalysis cuts are listed in Table III. The overall systematic error on the background fraction is 1.9%. Figure 5 shows the evolution of the background from triggering through to postanalysis cuts.

VII. RADIATIVE CORRECTIONS

In order to compare our experimental result for R with theoretical predictions based on quantum chromodynamics, we need the cross section for the annihilation of electron and positron into the single-photon intermediate state from which the final hadrons are produced, with no additional photons either virtual or radiated. This idealized nonradiative cross section is unphysical; the physical cross section will always contain higher-order amplitudes involving more virtual photons, as well as radiation of real photons by charged particles, especially the initial electron and positron. We describe in this section how we correct the measured cross section to account for the effect in the next order of α coming from the additional virtual and real photons, to obtain the idealized nonradiative cross section.

The radiative correction is expressed as a factor $(1+\delta)$ which, when multiplied by the idealized cross section σ_0, yields the observed cross section σ,

$$\sigma=\sigma_0(1+\delta_V+\delta_R)\ .$$

Here δ_V contains the effect of the interference of the lowest-order single-photon amplitude with the amplitude for an additional virtual photon, as well as the partially

TABLE III. Data composition for various postanalysis cuts on observed charged multiplicity n and energy E.

min n	min E (GeV)	Hadronic	Beam-wall[a]	QED[b]
5	3	0.973	0.023	0.004
6	3	0.981	0.017	0.002
7	3	0.986	0.014	$\ll$0.01
5	4	0.977	0.019	0.004
6	4	0.986	0.012	0.002
7	4	0.991	0.009	$\ll$0.01
5	5	0.980	0.016	0.004
6	5	0.989	0.009	0.002
7	5	0.993	0.007	$\ll$0.01

[a]Including beam-gas.
[b]Including ee, $\mu\mu$, and $\tau\tau$.

canceling cross section for radiation of very soft photons. The other term δ_R accounts for the cross section for real radiated photons of finite energies. The "virtual" correction may be further decomposed as

$$\delta_V=\delta_e+\delta_\mu+\delta_\tau+\delta_{\rm had}\ ,$$

where the last three terms are the contributions from the vacuum polarization loops containing muons, τ's, and quark-antiquark pairs.

For the terms not including δ_μ, δ_τ, or $\delta_{\rm had}$ we start with the expression of Bonneau and Martin[7] (using the notation of Jackson and Scharre[8]):

$$\sigma(W)=\sigma_0(W)\left[1+\frac{2\alpha}{\pi}\left[\frac{\pi^2}{6}-\frac{17}{36}\right]+t\ln\frac{k_{\rm min}}{E}+\frac{13t}{12}+t\int\left[1-\frac{k}{E}+\frac{k^2}{2E^2}\right]\times\frac{\sigma_0(W')}{\sigma_0(W)}\frac{dk}{k}\right].$$

Here $E=W/2$ is the single-beam energy, t is the equivalent radiator,

$$t=(2\alpha/\pi)[\ln(W^2/m_e{}^2)-1]\ ,$$

W' is the center-of-mass energy after radiation of the photon of energy k,

$$W'-2[E(E-k)]^{1/2}\ ,$$

and the integral is carried out between limits $k_{\rm min}$ and $k_{\rm max}$, which we will now discuss.

Following the procedure of Yennie, Frautschi, and Suura[9] we can multiply the infrared divergent terms in the integral by an exponential damping factor and let $k_{\rm min}=0$. Note that in order to evaluate the integral over k, we need to know the cross section at all energies W' less than the fixed W. Provided we separately account for the effect of nearby resonances in the cross section we can safely assume that R is approximately constant and replace $\sigma_0(W')$ by $\sigma_0(W)W^2/W'^2$. The Bonneau-Martin formula then reduces to

$$\delta_e=(2\alpha/\pi)(\pi^2/6-\tfrac{17}{36})+13t/12\ ,$$

$$\delta_R=t\int\left[1-\frac{k}{E}\right]^{-1}\frac{dk}{k}-t\int\left[1-\frac{k}{2E}\right]\frac{dk}{E-k}\ .$$

The upper limit $k_{\rm max}$ in the integrals is to be interpreted as the energy which must be radiated before the event is no longer accepted as a hadronic annihilation. In reality we do not work with a sharp cutoff, but rather a gradual decrease in our detection efficiency. Using the Monte Carlo simulation referred to earlier we determine the acceptance as a function of the maximum radiated energy $k_{\rm max}$, then replace the fixed $k_{\rm max}$ integral by a sum of piecewise integrals with weights chosen to reproduce the effect of the gradual variation in acceptance. The infrared divergence ($k\to0$) of the first integral is handled using the Yennie-Frautschi-Suura prescription.

For the lepton-loop terms δ_μ and δ_τ we use the expression of Berends and Gastmans[10] ($i=\mu,\tau$),

$$\delta_i=(2\alpha/\pi)[\tfrac{2}{3}\ln(W/m_i)-\tfrac{5}{9}]\ .$$

Through dispersion relations it is possible to relate the quark-loop term to the measured total cross section at lower energies:

$$\delta_{\rm had}(W)=-\frac{W^2}{2\pi^2\alpha}\int\sigma(W')\frac{dW'^2}{W^2-W'^2}\ ,$$

with the integral carried out between the threshold for hadron ($\pi\pi$) production and infinity. The integration is done numerically because of the presence of the ρ, ω, ϕ, and ψ resonances, and is rather insensitive to cross sections at very high energies.

The continuum data sample used for our measurement of R was obtained at e^+e^- center-of-mass energies above the $\Upsilon(3S)$ resonance and below the threshold for $B\bar{B}$ production. Before comparing with theory it is therefore necessary to subtract the contribution of the radiative tail of the $\Upsilon(3S)$ and lower resonances. Using the results of Sec. X, we calculate a contribution of 0.03 to the measured R, which we subtract.

Table IV shows the total radiative correction for the various postanalysis cuts. We assume that the dominant errors come from uncertainties in our treatment of the upper and lower limits of the k integration. From an evaluation of the sensitivity to reasonable variations in the hard photon acceptance function we estimate an error of 0.5%. An alternative infrared-cutoff procedure due to Berends and Kleiss[11] gives results for $1+\delta$ which are 98.7% of our value for a sharp $k_{\rm max}$, from which we estimate a 0.8% error in $1+\delta$. Adding the two errors in quadrature, we get 0.9% for the uncertainty in R due to the radiative correction.

VIII. LUMINOSITY

The luminosity $\mathscr{L}$, the electron-positron annihilation rate per unit cross section, depends on the beam currents,

TABLE IV. Corrected R and contributing factors for various postanalysis cuts on observed charged multiplicity n and energy E.

min n	min E (GeV)	ϵ	$1+\delta$	$R_{\rm obs}$[a]	R[b]
5	3	0.636	1.125	2.67	3.73±0.06
6	3	0.565	1.114	2.35	3.73±0.06
7	3	0.461	1.096	1.83	3.62±0.06
5	4	0.554	1.100	2.32	3.82±0.07
6	4	0.504	1.095	2.10	3.81±0.08
7	4	0.420	1.083	1.70	3.73±0.08
5	5	0.497	1.075	1.82	3.88±0.07
6	5	0.406	1.072	1.69	3.88±0.07
7	5	0.373	1.064	1.38	3.75±0.08

[a] $R_{\rm obs}=N(1-\beta)/(L\sigma_{\mu\mu})$.

[b] $R=R_{\rm obs}/[\epsilon(1+\delta)]$; errors include only counting statistics.

the area of intersection, and the circulation frequency. Since some of these latter quantities are not accurately measurable, we depend on the simultaneous observation of a reaction of known cross section, elastic e^+e^- (Bhabha) scattering, to determine the integrated luminosity $L=\int \mathscr{L}\,dt$ during our data runs. The calculation of this cross section requires only QED (except for a small hadronic term in the radiative corrections); in lowest order it is

$$\frac{d\sigma}{d\Omega}=\left[\frac{\alpha^2}{2W^2}\right]\left[\frac{q'^4+W^4}{q^4}+\frac{2q'^4}{q^2W^2}\frac{q'^4+q^4}{W^4}\right],$$

where $q^2=-W^2\sin^2\theta/2$, $q'^2=-W^2\cos^2\theta/2$, and θ is the positron scattering angle.

The CLEO detector records Bhabha scatters independently in three different angular ranges: in the small-angle lead and scintillator shower counters covering $39<\theta<70$ mrad, in the end-cap lead and proportional tube electromagnetic calorimeters covering $13°<\theta<29°$, and in the octant lead and proportional tube system covering $\theta>55°$. The small-angle luminosity monitors benefit from the large counting rate for elastic scatters at small angles and provide accurate run-to-run relative luminosities. However, because of their sensitivity to small alignment errors, they are not used for the absolute luminosity measurement. For this we use the much lower rate of large-angle Bhabha scatters in the octant shower detector. The end-cap Bhabha data at intermediate angles was used only as an occasional check of the long-term stability of the octant detector, and as a basis for estimating the systematic error in the luminosity measurement.

In the octant shower system we define a fiducial region for the shower centroids, covering 32% of the full solid angle. For an event to be identified as an elastic scatter, with or without accompanying radiated photons, the two highest-energy showers must be in opposite octants and must each deposit at least 2 GeV of energy. In addition, at least one shower centroid must be matched to a track in the cylindrical drift chamber inside the solenoid. If there are two tracks in the drift chamber, they must have an opening angle of at least 90°; events with more than two drift-chamber tracks are rejected. We estimate the efficiency of our Bhabha selection to be 97.2%. The background from $e^+e^-\to\gamma\gamma$, followed by photon conversion in the solenoid coil, is measured to be 1.7% by visual inspection of a sample of events.

The estimated 2.6% systematic error in the measurement of the Bhabha-scattering yield includes the following contributions added in quadrature: (1) 2.4% from the stability of the intercalibration of the octant and end-cap detection efficiencies, (2) 0.8% from the uncertainty in the $\gamma\gamma$ background measurement, (3) 0.3% from the uncertainty in the number of high-multiplicity events (e.g., $e^+e^-\gamma$ with converted photon) which fail the cuts, and (4) 0.4% from the octant-shower-counter calibration uncertainty.

The lowest-order QED Bhabha-scattering cross-section formula must be corrected for higher-order radiative effects. This is accomplished by a Monte Carlo simulation which includes real bremsstrahlung and virtual phonon and electron effects, along with separate estimates (Berends and Gastmans,[10] Berends and Komen[12]) of the muon, τ, and hadron vacuum-polarization contributions. The 2.3% systematic error in the radiative corrections includes in quadrature 1.0% from uncertainty in the cutoff procedures for high- and low-energy radiation, 1.5% from uncertainty in the vacuum-polarization terms, and 1.5% from uncertainty in the simulation of triggers for events with nearly collinear photon radiation by the outgoing electron or positron. The overall systematic error in the integrated luminosity $L=N_{\text{Bhabha}}/\sigma_{\text{Bhabha}}$ is then 3.5%.

IX. RESULT FOR R IN THE CONTINUUM

The CLEO measurment of R in the continuum is a by-product of the background measurements for studies of B-meson decays at the $\Upsilon(4S)$ resonance. It comprises runs taken at energies between the $\Upsilon(3S)$ resonance and the $B\bar{B}$ threshold, just below the $\Upsilon(4S)$, over four running periods. The average center-of-mass energy was $W=10.49$ GeV. A total of $N=4522$ accepted hadronic events were recorded for an integrated luminosity of $L=2055$ nb^{-1}.

The data from the four running periods are consistent within errors; the χ^2 with respect to the mean is 3.66 for 3 degrees of freedom. A small amount of data from a fifth running period (while the properties of the CLEO detector were undergoing modifications) was rejected as being inconsistent with the data from the other running periods at the same energies. Inclusion of the rejected data would have changed the measured R by 1.8%. We have therefore included (in quadrature) a 1.8% systematic error in R due to possible time variations in the detector acceptance.

Table IV shows the corrected value of R obtained for each of the nine combinations of postanalysis cuts in visible charged multiplicity and energy. The ultimate test of the validity of our acceptance and background calculations, the consistency of the R values, is apparently quite good. We take our final result for R to be the unweighted average of the nine determinations, with a statistical error obtained from the result of the least restrictive cuts. The standard deviation of the nine measurements is 2.1%, which we assign as a systematic error in the acceptance and background calculations, arising possibly from incorrectly simulated multiplicity and energy distributions for the hadronic annihilations, τ decays, and two-photon collisions. Table V summarizes the various contributions to the total 6.3% error estimate. No single source of error dominates.

The final result is then

$$R(10.49\text{ GeV})=\sigma_{\text{had}}/\sigma_{\mu\mu}=3.77\pm0.06\pm0.24\ .$$

Table VI shows the comparison of our measurement with results of other experiments performed at DORIS and CESR in the same energy region. The various measurements agree within their errors, which are rather similar. For all the measurements the errors are predominantly systematic; the accuracy of the mean of the measurements is probably not much better than the quoted accuracy of any one result.

Perturbative QCD makes a definite prediction for R.[18] In the modified minimal-subtraction $\overline{\text{MS}}$ scheme it is

TABLE V. Contributions to the systematic error in R.

Source	% error	See Sec.
Acceptance for postanalysis cuts	3.2	V
Acceptance for preanalysis requirements	2.2	V
Backgrounds	1.9	VI
Radiative corrections	0.9	VII
Luminosity	3.5	VIII
Time stability of acceptance	1.8	IX
Postanalysis cut consistency	2.1	IX
Net quadrature sum	6.3	

$$R=3(q_u{}^2+q_d{}^2+q_s{}^2+q_c{}^2)(1+\alpha_S/\pi+C_2\alpha_S{}^2/\pi^2+\cdots)$$

with $C_2=1.99-0.12\,N_f$, which implies $C_2=1.5$ between the $c\bar{c}$ and $b\bar{b}$ thresholds. For each flavor and color of quark-antiquark produced there is a term equal to the quark charge squared. The terms of higher order in the strong coupling α_S represent the effects of gluons. The coupling depends on energy W and the QCD scale constant Λ. A value of Λ near 120 MeV would imply R (10.5 GeV) = 3.49. The data are consistent with the QCD prediction. Although the experimental uncertainties are of the same size as the first-order correction ($\alpha_S/\pi=0.05$), the data do favor the full QCD prediction over the lowest-order parton prediction ($R=3.33$). The precision of the R measurements does not justify a calculation of the implied value of Λ.

X. THE NARROW Υ RESONANCES

The Υ $^3S_1$ 1^{--} bound states, denoted Υ(1S), Υ(2S), and Υ(3S), are observed in the total cross section for $e^+e^-\to$hadrons as narrow resonances at center-of-mass beam energies equal to their masses. The apparent width of the peaks is a consequence of the energy spread in the colliding beams, caused by synchrotron radiation. The rms center-of-mass energy spread δW is proportional to $W^2/\rho^{1/2}$, where ρ is the bending radius in the ring; in CESR it is expected to be $\delta W=4.1$ MeV at $W=10$ GeV. The intrinsic widths Γ of the three $^3S_1$ Υ states have been determined[19] to be less than 40 keV. Since at energies above the mass of a resonance it is possible for one of the incident $e^\pm$ to radiate enough energy to bring the e^+e^- center-of-mass energy down to the resonance mass, there will be a radiative tail in the cross section extending to higher energies above each resonance. In the following sections we describe the measurement of the resonant cross sections and the extraction of the resonance parameters, that is, the masses M and decay rates Γ_{ee} to the incident e^+e^- channel.

TABLE VI. Comparison of R measurements near $W=10$ GeV.

W (GeV)	R	Experiment
9.4	3.67±0.23±0.29	PLUTO[a]
9.5	3.73±0.16±0.28	DASP II[b]
9.4	3.8±0.7	DESY-Heidelberg[c]
9.1–9.5	3.34±0.09±0.18	LENA[d]
10.4	3.63±0.06±0.37	CUSB[e]
10.4	3.77±0.06±0.24	CLEO, this experiment

[a]Reference 13.
[b]Reference 14.
[c]Reference 15.
[d]Reference 16.
[e]Reference 17.

A. Measurements

Data used in the analysis of the narrow resonances were obtained over an 18-month period. These runs include but are not limited to those previously published.[20] For the Υ(1S), Υ(2S), and Υ(3S) energy scans we devoted integrated luminosities of 627, 1399, and 2037 nb^{-1}, respectively. We have excluded 39 nb^{-1} of data at the Υ(1S) and 107 nb^{-1} at the Υ(2S) because of problems of reproducibility of the measured cross sections; they serve as a basis for estimating the systematic error.

We select hadronic annihilation events by the same trigger, preanalysis filter, and postanalysis cuts as in the continuum measurement (Sec. IV) with one exception. After subtraction of the empirical flat nonresonant contribution, the resonance rate is background free. Therefore we are able to use less restrictive postanalysis cuts in visible charged multiplicity (≥ 3) and energy (≥ 3 GeV). The uncorrected visible cross sections N/L are shown in Fig. 6.

B. Resonance shapes

The observed annihilation cross section in the vicinity of a very narrow resonance may be written as

$$\sigma_{\rm vis}(W)=\int \sigma(w)G(W-w)dw\ ,$$

where $\sigma(w)$ is the physical cross section, essentially a δ function with a radiative tail, and $G(W-w)$ is the Gaussian beam-energy resolution function of rms width δW. The radiative correction is the same as discussed above for the continuum cross section, except for the form of the cross section. The radiation of hard photons may now be neglected, since anything except rather soft-photon radiation changes the center-of-mass collision energy enough to move away from the resonance. With only the soft-photon contribution we can write[8]

$$\sigma_{\rm vis}(W)=t\int dw\,G(W-w)\int \sigma_0(w')\left[\frac{2k}{W}\right]^t\frac{dk}{k}$$
$$+\delta_V\int \sigma(w)G(W-w)dw\ .$$

The w integration is over all energies; the k integration runs from 0 to $w/2$. Here, as before, w' is the center-of-mass energy after loss of a photon of energy k. Jackson and Scharre[8] invert the order of the double integral

$$\sigma_{\rm vis}(W)=\int \sigma_0(w)G_R(W-w)dw$$
$$+\delta_V\int \sigma(w)G(W-w)dw\ ,$$

where

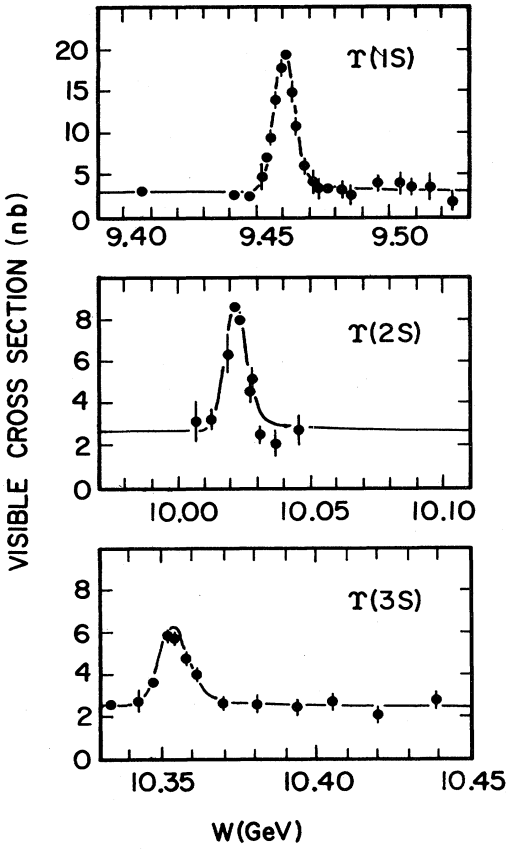

FIG. 6. The measured total cross section for $e^+e^- \rightarrow$hadrons in the vicinity of each of the first three Υ resonances, uncorrected for acceptance and backgrounds.

$$G_R(u)=t\int\left[\frac{2k}{W}\right]^t G(u')\frac{dk}{k}\ .$$

They derive an analytic approximation to $G_R(u)$ which is expected to be accurate to 0.2%. The visible resonance cross section (before acceptance correction) should therefore have an energy dependence determined by a G_R, a known function once δW is known, and a scale height determined by the radiation-free resonance cross section $\sigma_0(W)=A_0\delta(W-M)$.

We wish to extract the area A_0 of the radiation-free peak and the central mass M of the upsilon state from the experimental cross-section data as a function of W. To do this we make for each resonance a least squares fit to a nonresonant background proportional to W^{-2} (except for a 3% constant term to account for beam-wall contamination), plus a resonance form with the shape of G_R. The adjustable parameters in the fit are the beam-energy width δW and the desired A_0 and M parameters. The height of the nonresonant background is set by the measurement made at 10.49 GeV, discussed earlier. The fitted values of δW are plotted in Fig. 7. They are in excellent agreement with the expected W^2 dependence.

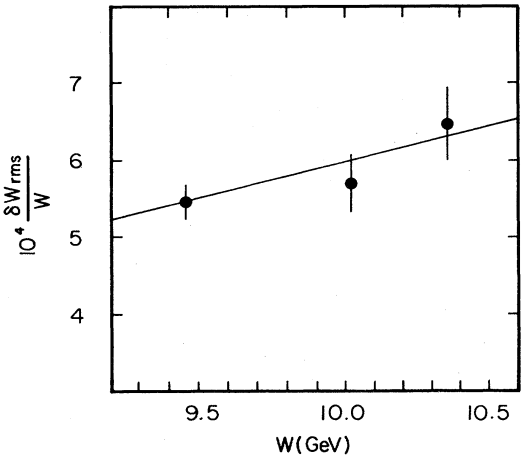

FIG. 7. The beam-energy dependence of the rms spread in beam energy as determined from fits to the measured width of the Υ resonances. The line shows the best linear fit.

C. Υ masses

The uncertainty in the masses is dominated by the error in the energy calibration of the CESR beams. The working energy scale is determined by the line integral of the magnetic field around the beam orbit. At the level of accuracy required here, it is a complicated function of magnetic field measurements made in several sample magnets powered in series with the storage ring magnets, the circulation frequency, and the currents in all the correction coils. Although the working energy scale is reproducible to better than 1 MeV, its absolute calibration is known internally to only 30 MeV.

The working energy scale is given an accurate calibration by means of a depolarization measurement. The circulating beams become automatically polarized by synchrotron radiation,[21] and can be resonantly depolarized by an external perturbing field of the right frequency. This frequency Ω is related to the $\gamma=E/m$ of the beam and to the electron anomalous magnetic moment by

$$\Omega=\omega_0[1+\gamma(g-2)/2]\ ,$$

where ω_0 is the orbit frequency. MacKay *et al.*[22] have made this calibration of the CESR working energy scale at the $\Upsilon(1S)$ energy, and have obtained a value of $9459.9\pm0.11\pm0.07$ MeV for the $\Upsilon(1S)$ mass. This mass for the $\Upsilon(1S)$ agrees well with the value obtained earlier with the same method by the VEPP4 group.[23] Using the MacKay *et al.* calibration of the working energy scale we determine the masses of the $\Upsilon(2S)$ and $\Upsilon(3S)$ with an accuracy of ±3 MeV, limited by uncertainty in the linearity of the working energy scale. Table VII shows our resulting Υ mass values.

D. Acceptance

The area A_0 under the intrinsic, radiationless resonance peak must now be corrected for the experimental acceptance ϵ; that is,

TABLE VII. Masses in MeV of Υ states from various experiments.

	$\Upsilon(1S)$	$\Upsilon(2S)$	$\Upsilon(3S)$
CESR[a]	9459.9±0.11±0.07	10021.4±0.3±3	10353.3±0.4±3
VEPP4[b]	9460.6±0.4	10023.8±0.5	10355.5±0.5
DORIS[c]	9462.0±3.0	10023.1±0.6	

[a]$M(1S)$ is from Ref. 22. $M(2S)$ and $M(3S)$ are obtained from our data using an energy scale fixed by the Ref. 22 measurement.
[b]Reference 23.
[c]Reference 24.

$$A_{\rm corr}=A_0/\epsilon\ .$$

The calculation of ϵ is the same as in the case of the continuum acceptance discussed above, except that (a) the Monte Carlo event generator must be changed to simulate the physics of Υ decays rather than the $q\bar{q}$ jets of the continuum, and (b) the postanalysis multiplicity and energy cuts are different.

We assume that Υ hadronic decays proceed through the following mechanisms.

(1) Decays to normal hadrons through the three-gluon intermediate state. The simulation forms the three gluon momenta using a QCD-motivated matrix element, then hadronizes the gluons much as the quarks are hadronized in the continuum $q\bar{q}$ simulation.

(2) Electromagnetic decays to normal hadrons through a virtual photon producing a quark-antiquark pair. These decays are simulated exactly as in the nonresonant continuum and should occur with a branching ratio which is just R times the branching ratio $B_{\mu\mu}$ into muon pairs.

(3) Radiative transition of a higher Υ to an intermediate $^3P_0$ or $^3P_2$ state followed by decay to normal hadrons by two gluons. The simulation of these two-jet decays can be combined with those of category (2).

(4) Radiative transition of a higher Υ to an intermediate $^3P_1$ state followed by decay to normal hadrons by three gluons or by a gluon and a quark-antiquark pair. These will be seen as three-jet decays and can be combined with category (1).

(5) Transition from a higher Υ to the $\Upsilon(1S)$ by emission of $\pi^+\pi^-$ or $\pi^0\pi^0$ pair. We treat this mode in combination with the three-jet categories (1) and (4).

The three-jet Monte Carlo implies an acceptance of 83% (varying slightly with the mass of the resonance), while the two-jet simulation gives 68%. Two-jet final states are more likely to be lost at small angles to the beam where the detector is not sensitive. The branching ratios for the $\Upsilon(1S)$, $\Upsilon(2S)$, and $\Upsilon(3S)$ into the five categories of modes are now known approximately.[19] For each Υ we take the net acceptance to be the mean, weighted by the appropriate branching ratios, of the acceptances calculated by the three-jet simulation (1, 4, and 5), and by the two-jet simulation (2 and 3). For the $\Upsilon(1S)$, $\Upsilon(2S)$, and $\Upsilon(3S)$ we use 12.4%, 6.8%, and 25.3% for the effective two-jet fractions, yielding 80%, 82%, and 82% for the net acceptances ϵ.

The estimated systematic errors follow closely the corresponding estimates for the continuum data discussed above, with some exceptions. The 1.3% uncertainty from the postanalysis cuts is smaller, because the resonance acceptance is higher and fewer events are lost. The preanalysis filter has a slightly higher error, 2.0%, because the visual scanning checks cannot be made with a pure sample of resonance events. From a study of the long-term stability of the acceptance during changes in the detection apparatus we estimate contributions to the systematic error of 2.9%, 8.0%, and 2.7% for the $\Upsilon(1S)$, $\Upsilon(2S)$, and $\Upsilon(3S)$, respectively.

There are no resonant backgrounds to be subtracted, and no corresponding error. However, since the nonresonant background was fixed in the cross-section fits, we must include an uncertainty in the continuum measurement. Because of the varying resonance-to-continuum ratios for the three Υ's, this introduces a varying relative error into the resonance fits: 0.6%, 1.5%, and 2.8%. We estimate an error of 0.8% in the radiative correction (from infrared cutoff ambiguities), and 3.5% in the luminosity monitoring. Combining errors in quadrature, we get 5.3%, 9.2%, and 5.8% for the systematic error in the measurement of $A_{\rm corr}$ for the three resonances.

E. Leptonic widths

The area $A_{\rm corr}$ under a resonance peak is related to the width Γ_{ee} for that state to decay to the input channel e^+e^-,

$$A_{\rm corr}=(6\pi/M^2)\Gamma_{ee}B_{\rm had}\ .$$

The hadronic branching ratio $B_{\rm had}$ follows from the mea-

TABLE VIII. Measured leptonic widths Γ_{ee} in keV.

	$\Upsilon(1S)$	$\Upsilon(2S)$	$\Upsilon(3S)$
This experiment	1.30±0.05±0.08	0.52±0.03±0.04	0.42±0.04±0.03
CUSB[a]	1.15±0.05±0.10	0.56±0.03±0.05	0.39±0.02±0.03
LENA[b]	1.23±0.10	0.53±0.07±0.06	
DASP II[c]	1.35±0.11	0.61±0.11±0.11	
PLUTO[d]	1.33±0.14		

[a]Reference 25.
[b]Reference 26.
[c]Reference 27.
[d]Reference 28.

TABLE IX. Measured excitation energies in MeV of Υ states [relative to the $\Upsilon(1S)$] compared with potential-model fits.[a]

State	This experiment	Martin	Eichten *et al.*	Buchmüller-Tye
$\Upsilon(2S)$	561.5±0.3±2	560	560	555
$\Upsilon(3S)$	893.6±0.4±2	890	898	890

[a]References 29 and 30.

TABLE X. Measured ratio of leptonic widths Γ_{ee} to leptonic width of the $\Upsilon(1S)$, compared with potential-model fits.[a]

State	This experiment	Martin	Eichten *et al.*	Buchmüller-Tye
$\Upsilon(2S)$	0.40±0.04±0.04	0.43	0.39	0.46
$\Upsilon(3S)$	0.32±0.03±0.02	0.28	0.27	0.32

[a]References 29 and 30.

surement of the muon-pair branching ratio $B_{\mu\mu}$ and lepton universality,

$$B_{\rm had}=1-3B_{\mu\mu}\ .$$

We therefore have

$$\Gamma_{ee}=(M^2/6\pi^2)A_{\rm corr}(1-B_{\mu\mu})^{-1}\ .$$

Along with our corrected, fitted results for $A_{\rm corr}$, we use the measured values[19] for $B_{\mu\mu}$ for the $\Upsilon(1S)$, $\Upsilon(2S)$, and $\Upsilon(3S)$: 3.3±0.5%, 1.8±1.0%, and 3.2±1.8%, respectively. The results for Γ_{ee} are given in Table VIII, along with values obtained in other experiments at DORIS and CESR. The agreement among the various measurements for each resonance is generally good.

F. Comparison with potential models

The mass differences among the $^3S_1$ Υ states have been derived from the same nonrelativistic potential models for the heavy quark-antiquark interaction that are used to relate the charmonium levels. A large variety of such models exist in the literature, some inspired by QCD,[29] with various levels of theoretical sophistication, others[30] completely empirical. All successful models agree that in the region of quark separation between 0.1 and 1.0 fm the potential has a distance behavior intermediate between the Coulombic behavior expected at small distances in perturbative QCD and the linear large-distance behavior expected from string models, that is, approximating log r or r raised to a small power (about 0.1). Table IX compares our data on mass differences with the predictions of some representative potential models.

These same potential models can also be used to make predictions of the leptonic widths of the Υ states. The Van Royen–Weisskopf formula[31] with the lowest-order QCD correction[32] is

$$\Gamma_{ee}=(16\alpha^2 q_b{}^2/M^2)\,|\,\psi(0)\,|^2(1-16\alpha_S/3\pi)$$

in terms of the $b\bar{b}$ wave function at zero separation, obtainable from the potential model solution. Because of the rather large (24%) QCD correction, one does not expect the predictions to be very accurate, although the predicted ratios of Γ_{ee} values for the three Υ states may be more reliable, since the QCD correction would then cancel approximately. In fact, the QCD-inspired potentials do rather well (Table X); the nonsingular empirical potentials tend to give low values for $|\,\psi(0)\,|^2$ and hence Γ_{ee}.

Probably the most reliable theoretical prediction for the leptonic width of the $\Upsilon(1S)$ is based on QCD sum rules.[33] One writes an energy moment of $R_b(W^2)$, the $b\bar{b}$ contribution to R, as both an asymptotic prediction from perturbative QCD and as an integral over bound states and continuum:

$$\int R_b(s)s^{-n-1}ds=A_n\frac{3q_b{}^2}{(4m_b{}^2)^n}$$
$$=9\pi\alpha^{-2}\left[\frac{\Gamma_{1See}}{M_{1S}{}^{2n+1}}+\frac{\Gamma_{2See}}{M_{2S}{}^{2n+1}}+\frac{\Gamma_{3See}}{M_{3S}{}^{2n+1}}+\int R_{b,\rm cont}(s)s^{-n-1}ds\right]\ .$$

A_n is a calculable constant depending on n and α_S. For large enough n the $\Upsilon(1S)$ contribution saturates the sum. Setting the right-hand sides equal for both $n=3$ and $n=4$, we can eliminate the dependence on the quark mass m_b and solve for Γ_{1See}. The most recent result[34] gives $\Gamma_{1See}=1.15\pm0.20$ keV, in good agreement with our data.

ACKNOWLEDGMENT

This work was supported in part by the National Science Foundation and the U. S. Department of Energy.

*Permanent address: LPC, College de France, Paris 75231 Cedex 05, France.

†Present address: Automatix, Inc., Billerica, MA 01821.

‡Present address: Singer-Kearfott, Little Falls, NJ 07424.

§Present address: University of Oklahoma, Norman, OK 73019.

**Present address: Lawrence Berkeley Laboratory, Berkeley, CA 94720.

††Present address: Fermilab, Batavia, IL 60510.

‡‡Present address: EP division, CERN, CH-1211 Geneva 23, Switzerland.

[1]D. Andrews *et al.*, Nucl. Instrum. Methods 211, 47 (1983); R. Ehrlich *et al.*, *ibid.* 211, 17 (1983).

[2]R. D. Field and R. P. Feynman, Phys. Rev. D 15, 2590 (1977); Nucl. Phys. B138, 1 (1978).

[3]J. D. Bjorken and S. J. Brodsky, Phys. Rev. D 1, 1416 (1970).

[4]S. Brandt *et al.*, Phys. Lett. 12, 57 (1964); S. Brandt and H. Dahmen, Z. Phys. C 1, 61 (1979); E. Farhi, Phys. Rev. Lett. 39, 1587 (1977).

[5]G. C. Fox and S. Wolfram, Phys. Rev. Lett. 41, 1581 (1978).

[6]C. A. Blocker *et al.*, Phys. Rev. Lett. 49, 1369 (1982).

[7]G. Bonneau and F. Martin, Nucl. Phys. B27, 381 (1971).

[8]J. D. Jackson and D. L. Scharre, Nucl. Instrum. Methods 128, 13 (1975).

[9]D. R. Yennie, S. C. Frautschi, and H. Suura, Ann. Phys. (N.Y.) 13, 379 (1961).

[10]F. A. Berends and R. Gastmans, in *Electromagnetic Interactions of Matter,* edited by A. Donnachie and G. Shaw (Plenum, London, 1978), p. 470.

[11]F. A. Berends and R. Kleiss, Nucl. Phys. B178, 141 (1981).

[12]F. A. Berends and G. J. Komen, Phys. Lett. 63B, 432 (1976).

[13]C. Berger *et al.*, Phys. Lett. 76B, 243 (1978).

[14]S. Weseler, Ph.D. thesis, University of Heidelberg, 1981.

[15]P. Bock *et al.*, Z. Phys. C 6, 125 (1980).

[16]B. Niczyporuk *et al.*, Z. Phys. C 15, 299 (1982).

[17]E. Rice, Ph.D. thesis, Columbia University, 1982.

[18]T. Appelquist and H. D. Politzer, Phys. Rev. D 12, 1404 (1975); E. C. Poggio *et al.*, *ibid.* 13, 1958 (1976); M. Dine and J. Sapirstein, Phys. Rev. Lett. 43, 668 (1979); K. G. Chetyrkin *et al.*, Phys. Lett. 85B, 277 (1979); W. Celmaster and R. J. Gonsalves, Phys. Rev. Lett. 44, 560 (1979).

[19]D. Andrews *et al.*, Phys. Rev. Lett. 50, 807 (1983).

[20]D. Andrews *et al.*, Phys. Rev. Lett. 44, 1108 (1980); 45, 219 (1980).

[21]A. A. Sokolov and I. M. Ternov, Dok. Akad. Nauk SSSR 8, 1052 (1963) [Sov. Phys. Dokl. 8, 1203 (1964)]; J. D. Jackson, Rev. Mod. Phys. 48, 417 (1976).

[22]W. W. MacKay *et al.*, paper C-262 submitted to the International Symposium on Photon and Lepton Interactions at High Energy, Cornell University, 1983 (unpublished).

[23]A. S. Artamonov *et al.*, Phys. Lett. 118B, 225 (1982).

[24]D. P. Barber *et al.*, paper C-309 submitted to the International Symposium on Lepton and Photon Interactions at High Energies, Cornell University, 1982 (unpublished); Report No. DESY 33-067 (unpublished).

[25]S. Youssef *et al.*, paper submitted to International Symposium on Lepton and Photon Interactions at High Energies, Cornell University, 1983 (unpublished).

[26]B. Niczyporuk *et al.*, Phys. Lett. 100B, 95 (1981); Z. Phys. C 17, 197 (1983).

[27]C. W. Darden *et al.*, Phys. Lett. 80B, 419 (1979).

[28]C. Berger *et al.*, Z. Phys. C 1, 343 (1979); 1, 243 (1978).

[29]E. Eichten *et al.*, Phys. Rev. D 17, 3090 (1978); 21, 203 (1980); G. Bhanot and S. Rudaz, Phys. Lett. 78B, 119 (1978); J. L. Richardson, *ibid.* 82B, 272 (1979); W. Buchmüller and S.-H. H. Tye, Phys. Rev. D 24, 132 (1981).

[30]M. Machacek and Y. Tomozawa, Ann. Phys. (N.Y.) 110, 407 (1978); C. Quigg and J. Rosner, Phys. Rev. D 23, 2625 (1981); A. Martin, Phys. Lett. 93B, 338 (1980); 100B, 511 (1981).

[31]R. Van Royen and V. F. Weisskopf, Nuovo Cimento 50A, 617 (1967).

[32]R. Barbieri *et al.*, Phys. Lett. 57B, 455 (1975); W. Celmaster, Phys. Rev. D 19, 1517 (1979).

[33]V. A. Novikov *et al.*, Phys. Rep. 41C, 1 (1978); M. A. Shifman, in *Proceedings of the 1981 International Symposium on Lepton and Photon Interactions at High Energies, Bonn,* edited by W. Pfeil (Physikalisches Institut, Universität Bonn, Bonn, 1981), p. 242.

[34]M. Voloshin and V. I. Zackharov, Phys. Rev. Lett. 45, 688 (1980).